THE JOURNAL OF PHYSICAL CHEMISTRY Letters

Letter

pubs.acs.org/JPCL

# Charge Trapping in Photovoltaically Active Perovskites and Related Halogenoplumbate Compounds

Ilya A. Shkrob*[,†] and Timothy W. Marin[†,‡]

[†]Chemical Sciences and Engineering Division, Argonne National Laboratory, 9700 South Cass Ave, Argonne, Illinois 60439, United States

[‡]Chemistry Department, Benedictine University, 5700 College Road, Lisle, Illinois 60532, United States

Supporting Information

**ABSTRACT:** Halogenoplumbate perovskites ($MeNH_3PbX_3$, where X is I and/or Br) have emerged as promising solar panel materials. Their limiting photovoltaic efficiency depends on charge localization and trapping processes that are presently insufficiently understood. We demonstrate that in halogenoplumbate materials the holes are trapped by organic cations (that deprotonate from their oxidized state) and $Pb^{2+}$ cations (as $Pb^{3+}$ centers), whereas the electrons are trapped by several $Pb^{2+}$ cations, forming diamagnetic lead clusters that also serve as color centers. In some cases, paramagnetic variants of these clusters can be observed. We suggest that charge separation in the halogenoplumbates resembles latent image formation in silver halide photography. Electron and hole trapping by lead clusters in extended dislocations in the bulk may be responsible for accumulation of trapped charge observed in this photovoltaic material.

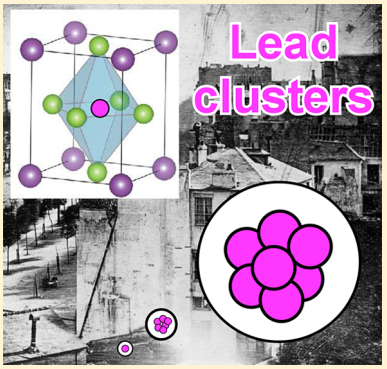


**SECTION:** Energy Conversion and Storage; Energy and Charge Transport

Halogenoplumbate perovskites (also known as organic−inorganic halide perovskites) with the structural formula of $MeNH_3PbX_3$ (where X is a halide(s)) have emerged[1−5] as extremely promising photovoltaic materials. Originally, it was believed that nanosize grains of these materials served as light antennas on mesoporous semiconductors,[4,6−8] but more recent research indicated that they perform equally well in thin layers[9,10] by rapidly directing photogenerated carriers[11] to interfaces,[12,13] where these photoinduced charges are extracted. The efficiency of the charge-separation process depends on the efficiency of charge trapping at the interfaces and by defects in the bulk.

We address the nature of such trapped charges. Because the photovoltaically active perovskites are a particular example of halogenoplumbate solids consisting of organic cations ($C^+$), we extended this study to related compounds that do not exhibit such properties. These reference compounds have the general chemical composition of $(CBr)_m{\cdot}PbX_2$ (X = Br, I), where $m$ = 1−3, and they include polycrystalline materials (including the compounds of methylammonium, tetramethylammonium, and pyridinium) and an ionic liquid[14] (of 1-butyl-3-methylimidazolium, $C_4$mim, for X = Br).[15,16] The details of the synthetic and analytical procedures are given in Section 1S in the Supporting Information. Solid materials yielded distinct crystalline phases, as demonstrated by X-ray diffraction (Figures 1S to 3S in the Supporting Information), and their chemical composition (Tables 1S and 2S in the Supporting Information) was established using nuclear magnetic resonance spectroscopy.

To study trapped charge centers in these materials, 3 MeV electrons from a van de Graaff accelerator or (for photoactive materials) 355 nm laser light were used as sources of radiation. The samples were irradiated at 77 K, and continuous-wave electron paramagnetic resonance (EPR) spectroscopy (at 9.45 GHz) was used to make structural inquiries. The details of sample preparation, irradiation regimes, and EPR spectroscopy are given in Section 2S of the Supporting Information. In the Figures the magnetic field is given in units of gauss (1 G = $10^{-4}$ T), and the first-derivative EPR spectra were obtained using the modulation of 2 G at 100 kHz. These EPR spectra were obtained at 50−250 K; as the temperature increases, radicals become mobile and reactions occur. Spin centers generated in Suprasil sample holders, such as $E_\gamma'$ centers (silica dangling bonds) and trapped hydrogen atoms and formyl radicals, are excluded from these EPR spectra.

Lead(II) is diamagnetic, but $Pb^{3+}$[17−22] and $Pb^{+}$[17,22−24] are paramagnetic cations that can be observed using EPR. Lead has only one naturally abundant magnetic (spin-1/2) isotope, $^{207}Pb$ with (21 at%), while even-mass isotopes have no nuclear spin. The typical hyperfine coupling constants (hfcc's) for $Pb^{3+}$ and $Pb^{+}$ are >10 kG and >1 kG (where 1 G = $10^{-3}$ T), respectively, and so these ions yield strong "central" resonance lines in their EPR spectra (corresponding to the even Pb isotopes) and weaker $^{207}Pb$ satellites that are typically impossible to observe

**Received:** February 24, 2014
**Accepted:** March 12, 2014
**Published:** March 12, 2014

  

in highly disordered materials due to inhomogeneous broadening. $Pb^{3+}$ centers ($6s^1$ species) have nearly isotropic $g$-tensors with principal values ~2, whereas $Pb^+$ centers ($6p^1$ species) have strongly axial $g$ tensors with principal values between 1 and 1.7.

Charge separation yields electron−hole pairs, and the released mobile carriers are subsequently trapped by preexisting defects in the bulk and by the surface of the crystallites. In alkali halides, the holes are trapped as $V_K$ centers ($X_2^{-\bullet}$ anions), while the electrons are trapped as F centers in anion vacancies.[25] In silver halides, the holes are trapped as $Ag^{2+}$ hole centers,[26−28] and the electrons are trapped by one or more $Ag^+$ cations in certain sites (e.g., by kinked edges at the surface and extended dislocations in the bulk).[28−30] Small surface clusters (such as $Ag_2^0$) can both trap electrons and inject holes from their excited state, and $Ag_2^+$ clusters (that serve as luminescence centers) can be observed using optically detected magnetic resonance.[28] Starting from four-atom silver clusters ($Ag_4^+$),[31,32] the growing nucleus can form the so-called latent image[33] that catalyzes reduction of AgX by certain chemical reagents (developers); this property is the chemical basis for black-and-white photography.[29,34]

This collective mode of electron trapping and cluster formation are not limited to silver halides. Even for the alkali compounds (such as oxide glasses and zeolites), clusters involving alkali atoms (with shared negative charge and, in paramagnetic clusters, spin) are formed, giving intense coloration to irradiated material.[35−37] In irradiated $PbX_2$ crystals, no $Pb^+$ centers have been observed,[38,39] suggesting nucleation of larger clusters or disproportionation yielding diamagnetic $Pb^0$ atoms that also form clusters.[38,40] Diatomic clusters (e.g., $Pb_2^{3+}$) have been observed in both irradiated $Pb^{2+}$-doped crystals, such as NaCl:$PbCl_2$,[41] and laser photoionization of single crystal $PbBr_2$ at 5−10 K.[42,43] In the latter system, these electron centers complement $Br_2^{-\bullet}$ hole centers. Warming of the irradiated $PbBr_2$ sample above 20 K caused recombination. Similar $Pb_2^{3+}$ centers were also observed in $PbCl_2$,[44−46] and both $PbF_2$ and $PbCl_2$ yield $Pb^{3+}$ centers.[43] There is also indirect spectroscopic evidence of larger paramagnetic lead clusters.[38,47] We stress that such direct evidence is presently lacking even for silver clusters in AgX crystals, although their involvement is beyond doubt.

We start our examination with EPR spectra of irradiated polycrystalline $PbX_2$ that are shown in Figure 1. The predominant feature is a strongly asymmetric line of a trapped hole center (with the unpaired electron density mainly on lead) that can be observed below 200 K. At 125−175 K, additional structure is observed (see Figure 4S in the Supporting Information) that has been variously interpreted as arising from different sites, impurity, or lead clusters.[38,44,47] In the following, we will refer to this center as the $Pb^{3+}$ center.[44] (We emphasize that in such centers the spin and excess charge density are spread over several anion shells.)[26,27,42,44] For every trapped-hole center, there is a complementary trapped-electron center that preserves charge neutrality. The import of these EPR spectra is that the released electrons are trapped (mainly) in an EPR-silent form.

Figure 2a,b exhibits EPR spectra of irradiated $Me_4NBr{\cdot}PbX_2$, which are polycrystalline solids. No $BrX^{-\bullet}$ species[42,48] or other halide-centered radicals are observed in these irradiated samples (Figure 2b), suggesting that halide anions do not trap charges in this system. The predominant feature in the EPR spectra for X = Br and X = I is the triplet from the $^{\bullet}CH_2NMe_3^+$ radical

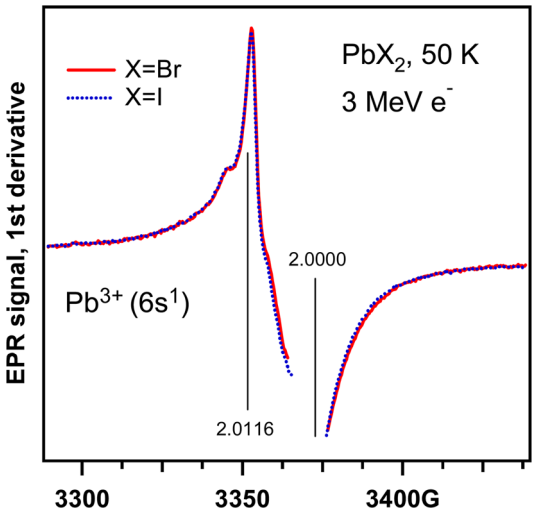


**Figure 1.** First-derivative EPR spectra of irradiated polycrystalline $PbBr_2$ and $PbI_2$ (see the legend). In both low-temperature solids, the $Pb^{3+}$ ($6s^1$) center with $g \approx 2$ is generated.

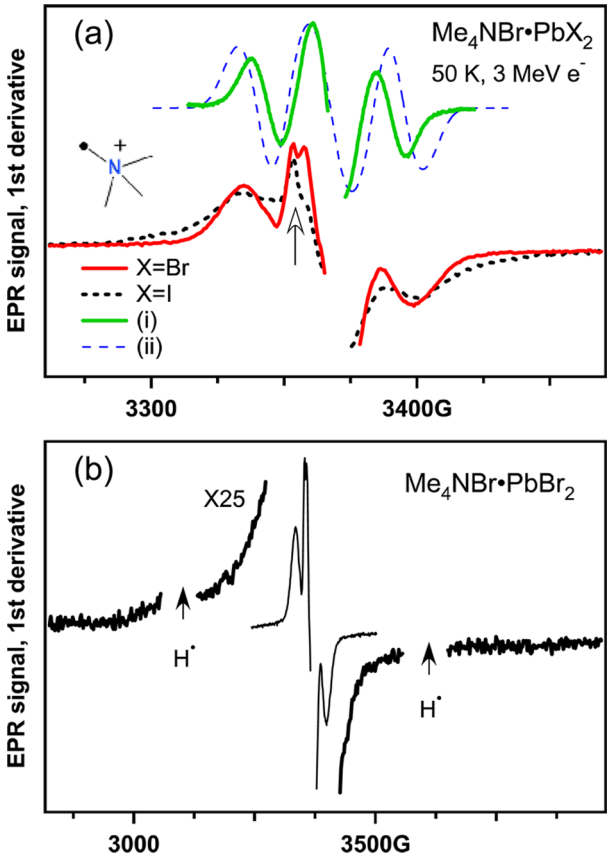


**Figure 2.** (a) First-derivative EPR spectra of irradiated $Me_4NBr{\cdot}PbX_2$ (X = Br, I), as indicated in the inset (observed at 50 K). Trace i is the EPR spectrum of the X = Br compound observed at 175 K. Trace ii is simulated EPR spectrum of gas-phase $^{\bullet}CH_2NMe_3^+$ radical cation using hfcc parameters calculated using density functional theory. (b) Wider field sweep for the X = Br compound is shown. There is no $Br_2^{-\bullet}$ anion or other resonance lines.

(Figure 2a). It is known from the previous research[49,50] that such H-loss radicals are the products of *hole* trapping: that is, electron detachment from the parent cation ($RH^+$) that yields a highly unstable intermediate ($RH^{2+\bullet}$) that promptly deproto-


dx.doi.org/10.1021/jz5004022 | J. Phys. Chem. Lett. 2014, 5, 1066−1071

nates yielding the $R^{+\bullet}$ radical cation and $H^{\delta+}A^{\delta-}$, where $A^-$ is the counteranion. Alternatively, this intermediate species can oxidize a neighboring anion. Radiation-induced oxidation of the cation apparently occurs in $Me_4NBr{\cdot}PbX_2$, but there is also a sharp feature, as indicated with an arrow. The location of this feature coincides with an identical feature in irradiated $PbX_2$ and is attributed to a $Pb^{3+}$ center (Figure 1). As the irradiated samples are warmed above 120 K (Figure 5S in the Supporting Information), this feature becomes broadened and "disappears" from the EPR spectra; the latter becomes precisely what one would expect for the $^{\bullet}CH_2NMe_3^+$ radical without interference from other species (Figure 2a). These spectral changes are reversible as the temperature is changed between 50 and 175 K. These results suggest that radiolysis yields two kinds of trapped hole centers: the $Pb^{3+}$ centers from the oxidation of $Pb^{2+}$ cations and H-loss radicals from oxidation of organic cations; no EPR-active trapped electron centers are observed.

For pyridinium compounds, $(C_5Y_6NBr)_2{\cdot}PbX_2$ (Y = H,D; X = Br,I), the EPR spectrum shown in Figure 6S (Supporting Information) is nearly identical to the one observed in the parent $PbX_2$ compound (Figure 1), suggesting that only $Pb^{3+}$ centers are formed. Indeed, such cations cannot deprotonate from their aliphatic arms when oxidized because they lack such groups; in this case only the halogenoplumbate anion is oxidized. Once again, the electron centers are not observed in the EPR spectra. What makes the latter observation remarkable is that in other solids this pyridinium cation can be easily reduced to the pyridinyl radical or $(C_5Y_6N)_2^{+\bullet}$ radical cations.[51] The fact that such reduced species are not observed in our EPR spectra indicates that the electrons are deeply trapped. Because neither the cations nor halides are involved, only lead cations can be involved in electron trapping.

A clue about the mode of this trapping is suggested by radiolysis of $C_4mim\ Br{\cdot}PbX_2$, which is the only compound that yielded an ionic liquid that can be quenched at low temperature as an amorphous solid. The predominant feature in the EPR spectrum of this glass (Figure 3) is a multiplet from the C-centered $R^{+\bullet}$ radicals generated via H atom loss in the aliphatic arm of the $C_4mim^+$ cation;[50] these radicals have been observed in other systems containing the $C_4mim^+$ cation. (See Figure 7S in the Supporting Information.)[49,52−54] In many of these systems, one also observes the 2-imidazolyl radical[53] or the corresponding C−C bound $\sigma^2\sigma^{1*}$ radical cation,[52−54] which is generated via electron trapping by the imidazolium cation. As in the case of pyridinium, no such trapped-electron centers are observed in the halogenoplumbates, once again suggesting deep electron trapping by $Pb^{2+}$ cations. As the temperature increases, the resonance lines of the $R^{+\bullet}$ radicals gradually disappear (Figure 3), and a very broad underlying signal becomes visible. Quick exposure of the material to 300 K softens the matrix, causing recombination of these organic radicals, and only the structureless singlet line is observed. This EPR spectrum (which corresponds to a Gaussian line with peak-to-peak spacing $\Delta B_{pp}$ of 58 G and $g$ = 2.0047) does not correspond to any organic or halogen radical but strongly resembles paramagnetic metal cluster centers observed in solid matrices (such as alkali electron centers in glasses,[35,36,55] and zeolites,[37] F-center colloids in alkali halides,[25] etc.) As the matrix softens, migration becomes possible and larger clusters can form; some of these can become paramagnetic through capture of the $Pb^{3+}$ center (which is suggested by the $g$ factor of the singlet line that exceeds that of the free electron). Concurrent with these spectral changes in EPR, the annealed glass develops intense black coloration that is suggestive of color center formation.

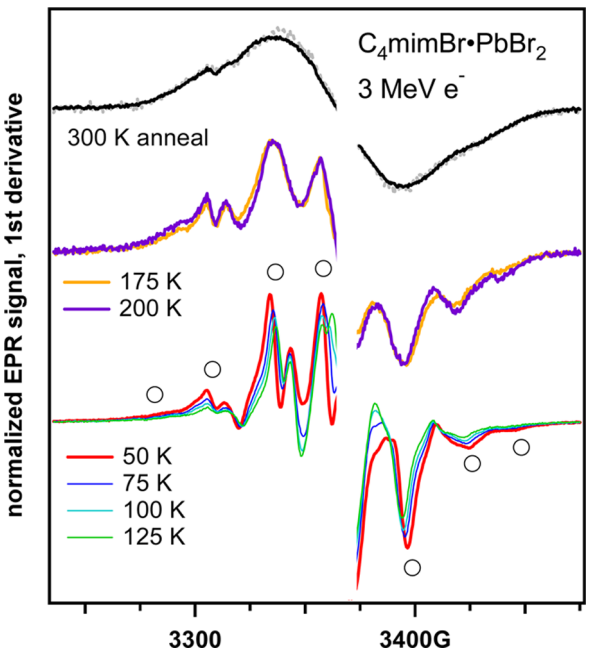


**Figure 3.** First-derivative EPR spectrum of irradiated frozen ionic liquid $C_4mimBr{\cdot}PbBr_2$. The sample temperature is indicated in the plot. Open circles indicate H-atom loss radicals in the aliphatic arm of the parent $C_4mim^+$ cation. After 30 s thermal anneal at 300 K, all organic radicals decay and the residual broad singlet (also seen in the 175 and 200 K traces) is observed without interference. In the top traces, the solid line corresponds to the EPR spectrum observed at 200 K, and the dashed line corresponds to the spectrum observed at 50 K.

We turn to the photovoltaic perovskite $MeNH_3Br{\cdot}PbBr_2$. From the preceding examination, one can expect the formation of the $^{\bullet}CH_2NH_3^+$ radical cation and the $Pb^{3+}$ center in this material. The former species can be generated on photoexcited $TiO_2$ anatase nanoparticles through oxidative decarboxylation of glycine ($HO_2CCH_2NH_3^+$).[56] As seen from Figure 4, irradiated perovskite yields this radical, too, albeit with more pronounced $g$-tensor anisotropy. Our modeling (Figure 4) indicates that to yield this EPR spectrum it is necessary to assume that the rotation of the $NH_3^+$ group is arrested in the crystal, but the HCNH dihedral angle is random in the ensemble. In addition to this $^{\bullet}CH_2NH_3^+$ radical cation, there is also a feature (indicated by an arrow, an asymmetric singlet line) that originates from the $Pb^{3+}$ center. As the temperature increases (Figure 8S in the Supporting Information), the signal from the $^{\bullet}CH_2NH_3^+$ radical cation becomes weaker (as the radicals recombine), and the underlying $Pb^{3+}$ center becomes more visible. Thus, charge trapping in this photovoltaic material is not significantly different from other halogenoplumbate compounds.

In these experiments, high-energy radiation was used to separate charges, and it is reasonable to ask what reactions occur under milder excitation conditions. To answer this question, we used 355 nm laser light to photoirradiate frozen $MeNH_3Br{\cdot}PbBr_2$ and $C_4mimBr{\cdot}PbBr_2$ at 77 K. The EPR spectra shown in Figure 5 were observed at 50 K; no paramagnetic species were observed at 300 K. This EPR signal was observed only at high photon fluences. Visually, the formation of this EPR signal coincided with changing of the color of the crystal surface from orange to black, which strongly


dx.doi.org/10.1021/jz5004022 | J. Phys. Chem. Lett. 2014, 5, 1066−1071

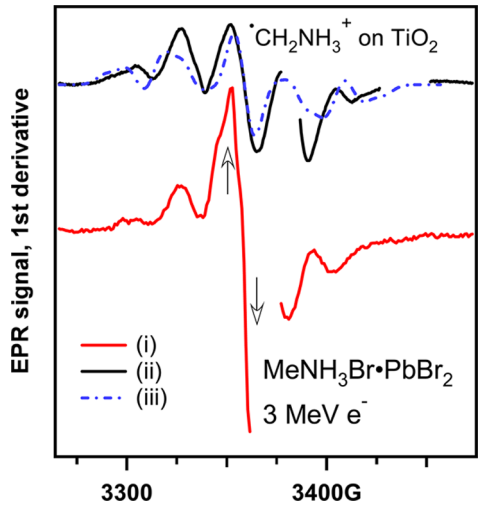


**Figure 4.** First-derivative EPR spectrum of irradiated perovskite crystals (trace i). Trace ii is the EPR spectrum of $^{\bullet}CH_2NH_3^+$ on illuminated anatase nanoparticles; this radical cation is generated via photooxidation of glycine at pH 1. Trace iii is simulated EPR spectrum of the ensemble of conformationally frozen $^{\bullet}CH_2NH_3^+$ species. The arrows indicate the overlapping signal from the $Pb^{3+}$ center.

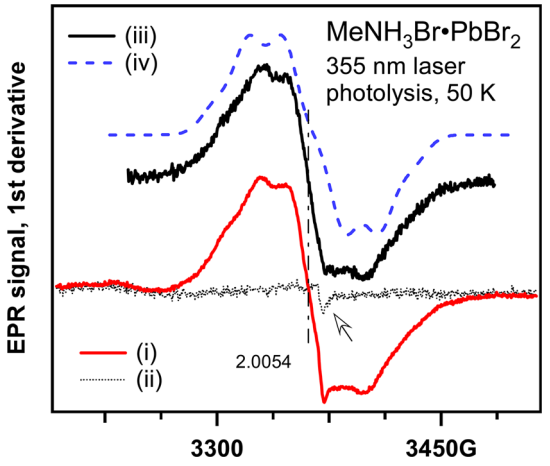


**Figure 5.** First-derivative EPR spectrum of photoirradiated crystalline perovskite (trace i). Trace ii was obtained after annealing the sample at 200 K and cooling it back to 50 K. Trace iii is the difference trace, and trace iv is simulated EPR spectrum of $^{\bullet}CH_2NH_3^+$ radical assuming free rotation in the $NH_3^+$ group and significant line broadening.

implicates color center formation. As seen from Figure 5, after the subtraction of the background the EPR spectrum is almost featureless. This EPR spectrum can be simulated as originating entirely from the $^{\bullet}CH_2NH_3^+$ radical cation, in which the $NH_3$ group rotates freely, assuming that there is significant broadening of the lines. While it is possible that $^{\bullet}CH_2NH_3^+$ radical cations generated in radiolysis and laser photolysis are trapped at different sites, it seems unlikely that such a radical would have $g$ factor of 2.0067. (As in other systems, the $g$ factor for this radical is 2.0028.) It appears more likely that the resolved features seen in Figure 5 originate from the same $^{\bullet}CH_2NH_3^+$ radical cation that is observed in radiolysis, but the resonance lines overlap with a broad resonance line similar to the one observed in Figure 4. This resonance line also overlaps with the line of the $Pb^{3+}$ center that is seen in the irradiated sample annealed at 200 K. We suggest that in both of these cases the broad line originates from paramagnetic $Pb^0$ clusters sharing an unpaired electron and the same species account for the black coloration. A broad EPR line and color center formation were also observed in low-temperature photoirradiation of $C_4mimBr{\cdot}PbBr_2$. (See Figure 9S in the Supporting Information.)

These EPR results suggest that radiation-induced charge separation in organic halogenoplumbates, including photoactive perovskites, occurs through the formation of oxidized (and deprotonated) organic cations and the $Pb^{3+}$ centers, while the electrons are collectively trapped by several $Pb^{2+}$ cations. The resulting clusters are EPR-silent (as is also the case in other systems of this type, including the AgX and $PbX_2$ crystals), but in some cases it is possible to observe paramagnetic variants. Charge-trapping processes in these halogenoplumbates appear to resemble the ones that are involved in the initiation of latent image formation in photography.[29] The resulting metallic clusters must be similar to atomic clusters in other halide crystals; in particular, these are relatively small clusters, as suggested by the absence of the Dysonian resonance lines in the EPR spectra of their paramagnetic counterparts.

This mode of charge localization has direct bearing on the unusual efficiency of photoinduced charge separation in halogenoplumbate perovskites: rapid trapping of the electrons by $Pb^{2+}$ ions (in full analogy to the same process in AgX microcrystals) can potentially account for suppressed recombination. The formation of lead clusters in dislocations and charge (e.g., hole) trapping by such clusters may also be responsible for the unaccounted accumulation of trapped charge in the perovskite cells reported by Kim et al.[57] The formation of lead clusters would be in agreement with electronic structure calculations, suggesting that the bottom of the conduction band is dominated by Pb 6p states.[58−60] Such clusters can facilitate exciton dissociation and interfacial charge transfer to the p- and n-conducting materials.

We also note that Pb 4f signatures of metallic lead have been reported in two recent X-ray photoemission spectroscopy studies of $CH_3NH_3X{\cdot}PbI_2$ (X = Cl, I).[61,62] Our EPR results rationalize the formation of such clusters as effects of radiolysis by intense beams of hard X-rays.

## ■ ASSOCIATED CONTENT

### Ⓢ Supporting Information

Synthetic and experimental detail. $^1H$ NMR data for $(CBr)_m{\cdot}PbX_2$ (X = I, Br) compounds. Mole fraction $m$ of organic cations ($C^+$) in $(CBr)_m{\cdot}PbX_2$ (X = I, Br) compounds as determined by quantitative $^1H$ NMR analysis. $g$-Factors and isotropic hyperfine coupling constants for selected radicals. X-ray diffractograms (Cu K$\alpha$) of polycrystalline samples. First-derivative EPR spectra of the $Pb^{3+}$ center in irradiated polycrystalline $PbI_2$, irradiated $Me_4NBr{\cdot}PbI_2$ and $Me_4NBr{\cdot}PbI_2$, irradiated $(C_5X_6Br){\cdot}PbBr_2$, irradiated frozen ionic liquid $C_4mimBr{\cdot}PbBr_2$, crystalline perovskite $MeNH_3Br{\cdot}PbBr$, and photoirradiated frozen ionic liquid $C_4mimBr{\cdot}PbBr_2$. This material is available free of charge via the Internet at http://pubs.acs.org.

## ■ AUTHOR INFORMATION

### Corresponding Author

*Tel: (630) 252-9516. E-mail: shkrob@anl.gov.

### Notes

The authors declare no competing financial interest.

## ■ ACKNOWLEDGMENTS

We thank J. Muntean, D. Quigley, and R. Lowers for technical support and S. Skanthakumar and Geng Bang Jin for X-ray characterization of crystalline samples. This work was supported by the US-DOE Office of Science, Division of Chemical Sciences, Geosciences and Biosciences under contract nos DE-AC02-−06CH11357. Programmatic support via a DOE SISGR grant "An Integrated Basic Research Program for Advanced Nuclear Energy Separations Systems Based on Ionic Liquids" is gratefully acknowledged.

## ■ REFERENCES

(1) Kojima, A.; Teshima, K.; Shirai, Y.; Miyasaka, T. Organometal Halide Perovskites as Visible-Light Sensitizers for Photovoltaic Cells. *J. Am. Chem. Soc.* **2009**, *131*, 6050−6051.

(2) Park, N.-G. Organometal Perovskite Light Absorbers toward a 20% Efficiency Low-Cost Solid-State Mesoscopic Solar Cell. *J. Phys. Chem. Lett.* **2013**, *4*, 2423−2429.

(3) Burschka, J.; Pellet, N.; Moon, S.-J.; Humphry-Baker, R.; Gao, P.; Nazeeruddin, M. K.; Grätzel, M. Sequential Deposition as a Route to High-Performance Perovskite-Sensitized Solar Cells. *Nature (London)* **2013**, *499*, 316−320.

(4) Kim, H.-S.; Lee, J.-W.; Yantara, N.; Boix, P. P.; Kulkarni, S. A.; Mhaisalkar, S.; Grätzel, M.; Park, N.-G. High Efficiency Solid-State Sensitized Solar Cell-Based on Submicrometer Rutile $TiO_2$ Nanorod and $CH_3NH_3PbI_3$ Perovskite Sensitizer. *Nano Lett.* **2013**, *13*, 2412−2417.

(5) Heo, J. H.; Im, S. H.; Noh, J. H.; Mandal, T. N.; Lim, C.-S.; Chang, J. A.; Lee, Y. H.; Kim, H.; Sarkar, A.; Nazeeruddin, M. K.; et al. I. Efficient Inorganic−Organic Hybrid Heterojunction Solar Cells Containing Perovskite Compound and Polymeric Hole Conductors. *Nat. Photonics* **2013**, *7*, 486−491.

(6) Edri, E.; Kirmayer, S.; Cahen, D.; Hodes, G. High Open-Circuit Voltage Solar Cells Based on Organic−Inorganic Lead Bromide Perovskite. *J. Phys. Chem. Lett.* **2013**, *4*, 897−902.

(7) Zhao, Y.; Zhu, K. Charge Transport and Recombination in Perovskite $(CH_3NH_3)PbI_3$ Sensitized $TiO_2$ Solar Cells. *J. Phys. Chem. Lett.* **2013**, *4*, 2880−2884.

(8) Lee, M. M.; Teuscher, J.; Miyasaka, T.; Murakami, T. N.; Snaith, H. J. Efficient Hybrid Solar Cells Based on Meso-Superstructured Organometal Halide Perovskites. *Science* **2012**, *338*, 643−647.

(9) Snaith, H. J. Perovskites: The Emergence of a New Era for Low-Cost, High-Efficiency Solar Cells. *J. Phys. Chem. Lett.* **2013**, *4*, 3623−3630.

(10) Liu, M.; Johnston, M. B.; Snaith, H. J. Efficient Planar Heterojunction Perovskite Solar Cells by Vapour Deposition. *Nature (London)* **2013**, *501*, 395−398.

(11) Marchioro, A.; Brauer, J. C.; Teuscher, J.; Grätzel, M.; Moser, J.-E. Photoinduced Processes in Lead Iodide Perovskite Solid-State Solar Cells. *Proc. SPIE* **2013**, *8811*, 881108 (6 pages)..

(12) Xing, G.; Mathews, N.; Sun, S.; Lim, S. S.; Lam, Y. M.; Grätzel, M.; Mhaisalkar, S.; Sum, T. C. Long-Range Balanced Electron and Hole-Transport Lengths in Organic-Inorganic $CH_3NH_3PbI_3$. *Science* **2013**, *342*, 344−347.

(13) Zhao, Y.; Nardes, A. M.; Zhu, K. Solid-State Mesostructured Perovskite $Ch_3nh_3pbi_3$ Solar Cells: Charge Transport, Recombination, and Diffusion Length. *J. Phys. Chem. Lett.* **2014**, *5*, 490−494.

(14) Hallett, J. P.; Welton, T. Room-Temperature Ionic Liquids: Solvents for Synthesis and Catalysis. 2. *Chem. Rev.* **2011**, *111*, 3508−3576.

(15) Coleman, F.; Feng, G.; Murphy, R. W.; Nockemann, P.; Seddon, K. R.; Swadźba-Kwaśny, M. Lead(II) Chloride Ionic Liquids and Organic/Inorganic Hybrid Materials − a Study of Chloroplumbate(II) Speciation. *Dalton Trans.* **2013**, *42*, 5025−5035.

(16) Thirumurugan, A.; Rao, C. N. R. Supramolecular Organization in Lead Bromide Salts of Imidazolium-Based Ionic Liquids. *Cryst. Growth Des.* **2008**, *8*, 1640−1644.

(17) Solntsev, V. P.; Mashkovtsev, R. I.; Davydov, A. V.; Tsvetkov, E. G. EPR Study of Coordination of Ag and Pb Cations in $BaB_2O_4$ Crystals and Barium Borate Glasses. *Phys. Chem. Minerals* **2008**, *35*, 311−320.

(18) Bilbe, R. M.; Nicholls, J. E.; Davies, J. J. Electron Paramagnetic Resonance Investigation of Pb- and Ge-Doped Cdte. *v* **1984**, *121*, 339−344.

(19) Abraham, M. M.; Boatner, L. A.; Rappaz, M. Novel Measurement of Hyperfine Interactions in Solids: $^{207}Pb^{3+}$ in $YPO_4$ and $LuPO_4$. *Phys. Rev. Lett.* **1980**, *45*, 839−842.

(20) Hosono, H.; Nishii, J.; Kawazoe, H.; Kanazawa, T.; Ametani, K. EPR Spectra of $Pb^{3+}$ and $Ag^0$ in Glass. *J. Phys. Chem.* **1980**, *84*, 2316−2319.

(21) Morton, J. R.; Preston, K. F.; Strach, S. J. Electron Paramagnetic Resonance Spectra of γ-Irradiated Germanium, Tin, and Lead Tetraacetates. *J. Phys. Chem.* **1979**, *83*, 853−855.

(22) Baranov, P. G.; Khramtsov, V. A. EPR Study of Impurity Colour Centres in P-State in Alkali Halides. *Phys. Status Solidi B* **1980**, *153*, 153−161.

(23) Goovaerts, E.; Nistor, S. V.; Schoemaker, D. Electron-Spin Resonance of a Complex $Pb^+$ $(6p^1)$ Defect in Alkali Halides. *Phys. Rev. B* **1983**, *28*, 3712−3717.

(24) Heynderickx, I.; Goovaerts, E.; Schoemaker, D. Hyperfine Behavior of the Laser-Active $Tl^0(I)$ Center in Alkali-Halides. *Solid State Commun.* **1985**, *55*, 877−880.

(25) Hayes, W.; Stoneham, A. M. *Defects and Defect Processes in Nonmetallic Solids*; Dover Publications: Mineola, NY, 2004.

(26) Baranov, P. G.; Romanov, N. G.; Poluektov, O. G.; Schmidt, J. Self-Trapped Excitons in Ionic-Covalent Silver Halide Crystals and Nanostructures: High-Frequency EPR, ESE, ENDOR and ODMR Studies. *Appl. Magn. Reson.* **2010**, *39*, 453−486.

(27) Bennebroek, M. T.; v. Duijn-Arnold, A.; Schmidt, J.; Poluektov, O. G.; Baranov, P. G. Self-Trapped Hole in Silver Chloride Crystals: A Pulsed EPR and ENDOR Study at 95 Ghz. *Phys. Rev. B* **2002**, *66*, 054305-1−054305-8.

(28) Eachus, R. S.; Marchetti, A. P.; Muenter, A. A. The Photophysics of Silver Halide Imaging Materials. *Annu. Rev. Phys. Chem.* **1999**, *50*, 117−144.

(29) Tani, T. *Photographic Science: Advances in Nanoparticles, J-Aggregates, Dye Sensitization, and Organic Devices*; Oxford University Press: New York, 2011.

(30) Tani, T. Physics of the Photographic Latent Image. *Phys. Today* **1989**, *42*, 36−41.

(31) Fayet, P.; Granzer, F.; Hegenbart, G.; Moisar, E.; Pischel, B.; Woste, L. Latent-Image Generation by Deposition of Monodisperse Silver Clusters. *Phys. Rev. Lett.* **1985**, *55*, 3002−3004.

(32) Fayet, P.; Granzer, F.; Hegenbart, G.; Moisar, E.; Pischel, B.; Woste, L. The Role of Small Silver Clusters in Photography. *Z. Phys. D* **1986**, *3*, 299−302.

(33) Mitchell, J. W. Photographic Sensitivity. *Rep. Prog. Phys.* **1957**, *20*, 433−515.

(34) Tani, T. *Photographic Sensitivity: Theory and Mechanisms*; Oxford University Press: New York, 1995.

(35) Griscom, D. L. ESR and Optical Studies of Alkali-Associated Trapped-Electron Centers in Alkali Borate Glasses Irradiated at 77 K. *J. Non-Cryst. Solids* **1971**, *6*, 275−282.

(36) Taylor, P. C.; Griscom, D. L. Toward a Unified Interpretation of ESR Trapped-Hole Centers in Irradiated Borate Compounds and Glasses. *J. Chem. Phys.* **1971**, *55*, 3610−3618.

(37) Blake, N. P.; Stucky, G. D. Alkali-Metal Clusters as Prototypes for Electron Solvation in Zeolites. In *Inclusion Chemistry with Zeolites: Nanoscale Materials by Design. Topics in Inclusion Science*; Herron, N., Corbin, D. R., Eds.; Springer Science and Business Media: Dordrecht, The Netherlands, 1995; Vol. *6*, pp 299−324.

(38) Arends, J.; Verwey, J. F. ESR on UV Irradiated Lead Halides at 80 K. *Phys. Status Solidi B* **1967**, *23*, 137−145.

(39) Patankar, A. V.; Schneider, E. E. ESR of Colour Centres in γ-Irradiated Planar Lead Halides. *J. Phys. Chem. Solids* **1966**, *27*, 575−579.

(40) Novosad, I. S.; Novosad, S. S.; Bordun, O. M.; Pashuk, I. P. Thermally Stimulated and Photoinduced Depolarization Processes in $PbI_2$ Crystals. *Inorg. Mater.* **2006**, *42*, 226−230.
(41) Heynderickx, I.; Goovaerts, E.; Schoemaker, D. Electron-Spin-Resonance Study of $Pb_2^{3+}$ Dimer Centers in NaCl:$PbCl_2$. *Phys. Rev. B* **1987**, *36*, 1843−1852.
(42) Iwanaga, M.; Azuma, J.; Shirai, M.; Tanaka, K.; Hayashi, T. Self-Trapped Electrons and Holes in $PbBr_2$ Crystals. *Phys. Rev. B* **2002**, *65*.
(43) Iwanaga, M.; Hayashi, T. Exciton-Relaxation Dynamics in Lead Halides. *J. Lumin.* **2003**, *2003*, 663−668.
(44) Iwanaga, M.; Shirai, M.; Tanaka, K.; Hayashi, T. Self-Trapped States and Related Luminescence in $PbCl_2$ Crystals. *Phys. Rev. B* **2002**, *66*, 064304-1−064304-8.
(45) Hirota, T.; Fujita, T.; Kazumata, Y. Electron Spin Resonance Study of Centers Formed in Γ-Irradiated $PbCl_2$ Crystals. *Jpn. J. Appl. Phys.* **1993**, *32*, 4674−4679.
(46) Nistor, S. V.; Goovaerts, E.; Schoemaker, D. Direct Observation of Electron Self-Trapping in $PbCl_2$ Crystals. *Phys. Rev. B* **1993**, *48*, 9575−9580.
(47) Gruijter, W. C. D.; Kerssen, J. Luminescence of $PbCl_2$ and $PbBr_2$ Single Crystals Ii. Luminescence and EPR of UV Irradiated Crystals. *J. Solid State Chem.* **1972**, *5*, 467−476.
(48) Shkrob, I. A.; Marin, T. W.; Crowell, R. A.; Wishart, J. F. Photo- and Radiation- Chemistry of Halide Anions in Ionic Liquids. *J. Phys. Chem. A* **2013**, *117*, 5742−5756.
(49) Shkrob, I. A.; Chemerisov, S. D.; Wishart, J. F. The Initial Stages of Radiation Damage in Ionic Liquids and Ionic Liquid-Based Extraction Systems. *J. Phys. Chem. B* **2007**, *111*, 11786−11793.
(50) Shkrob, I. A.; Wishart, J. F. Free Radical Chemistry in Room-Temperature Ionic Liquids. In *Encyclopedia of Radicals in Chemistry, Biology and Materials*; Chatgilialoglu, C., Studer, A., Eds.; John Wiley & Sons, Ltd.: Chichester, U.K., 2012; pp 433−448.
(51) Shkrob, I. A.; Marin, T. W.; Hatcher, J. L.; Cook, A. R.; Szreder, T.; Wishart, J. F. Radiation Stability of Cations in Ionic Liquids. 2. Improved Radiation Resistance through Charge Delocalization in 1-Benzylpyridinium. *J. Phys. Chem. B* **2013**, *117*, 14385−14399.
(52) Shkrob, I. A.; Wishart, J. F. Charge Trapping in Imidazolium Ionic Liquids. *J. Phys. Chem. B* **2009**, *113*, 5582−5592.
(53) Shkrob, I. A.; Marin, T. W.; Luo, H.; Dai, S. Radiation Stability of Cations in Ionic Liquids. 1. Alkyl and Benzyl Derivatives of 5-Membered Ring Heterocycles. *J. Phys Chem. B* **2013**, *117*, 14372−14384.
(54) Shkrob, I. A.; Marin, T. W.; Chemerisov, S. D.; Hatcher, J. L.; Wishart, J. F. Radiation Induced Redox Reactions and Fragmentation of Constituent Ions in Ionic Liquids. 2. Imidazolium Cations. *J. Phys. Chem. B* **2011**, *115*, 3889−3902.
(55) Shkrob, I. A.; Tadjikov, B. M.; Trifunac, A. D. Magnetic Resonance Studies on Radiation-Induced Point Defects in Mixed Oxide Glasses. I. Spin Centers in $B_2O_3$ and Alkali Borate Glasses. *J. Non-Cryst. Solids* **2000**, *262*, 6−34.
(56) Shkrob, I. A.; Chemerisov, S. D. Light Induced Fragmentation of Polyfunctional Carboxylated Compounds on Hydrated Metal Oxide Particles: From Simple Organic Acids to Peptides. *J. Phys. Chem. C* **2009**, *113*, 17138−17150.
(57) Kim, H.-S.; Mora-Sero, I.; Gonzalez-Pedro, V.; Fabregat-Santiago, F.; Juarez-Perez, E. J.; Park, N.-G.; Bisquert, J. Mechanism of Carrier Accumulation in Perovskite Thin-Absorber Solar Cells. *Nat. Commun.* **2013**, *4*, 2242-1−2242-6.
(58) Wang, Y.; Gould, T.; Dobson, J. F.; Zhang, H.; Yang, H.; Yao, X.; Zhao, H. Density Functional Theory Analysis of Structural and Electronic Properties of Orthorhombic Perovskite $CH_3NH_3PbI_3$. *Phys. Chem. Chem. Phys.* **2014**, *16*, 1424−1429.
(59) Baikie, T.; Fang, Y.; Kadro, J. M.; Schreyer, M.; Wei, F.; Mhaisalkar, S. G.; Graetzel, M.; Whitec, T. J. Synthesis and Crystal Chemistry of the Hybrid Perovskite $(CH_3NH_3)PbI_3$ for Solid-State Sensitised Solar Cell Applications. *J. Mater. Chem. A* **2013**, *1*, 5628−5641.
(60) Mosconi, E.; Amat, A.; Nazeeruddin, M. K.; Grätzel, M.; De Angelis, F. First-Principles Modeling of Mixed Halide Organometal Perovskites for Photovoltaic Applications. *J. Phys. Chem. C* **2013**, *117*, 13902−13913.
(61) Lindblad, R.; B, D.; Park, B.; Oscarsson, J.; Gorgoi, M.; Siegbahn, H.; Odelius, M.; Johansson, E. M. J.; Rensmo, H. Electronic Structure of $TiO_2/CH_3NH_3PbI_3$ Perovskite Solar Cell Interfaces. *J. Phys. Chem. Lett.* **2014**, *5*, 648−653.
(62) Conings, B.; Baeten, L.; De Dobbelaere, C.; D'Haen, J.; Manca, J.; H.-G., B. Perovskite-Based Hybrid Solar Cells Exceeding 10% Efficiency with High Reproducibility Using a Thin Film Sandwich Approach. *Adv. Mater.* **2013**, DOI: 10.1002/adma.201304803.